Available online at www.sciencedirect.com
SCIENCE DIRECT®
Journal of Contaminant Hydrology 76 (2005) 251–277
JOURNAL OF Contaminant Hydrology
www.elsevier.com/locate/jconhyd

Numerical methods for improving sensitivity analysis and parameter estimation of virus transport simulated using sorptive–reactive processes

Gilbert Barth[a,*], Mary C. Hill[b]

[a]S.S. Papadopulos and Associates, 1877 Broadway, Suite 703, Boulder, CO 80305, United States
[b]U.S. Geological Survey, 3215 Marine St., Boulder, CO 80303-1066, United States

Received 24 October 2003; received in revised form 27 September 2004; accepted 22 October 2004

Abstract

Using one- and two-dimensional homogeneous simulations, this paper addresses challenges associated with sensitivity analysis and parameter estimation for virus transport simulated using sorptive–reactive processes. Head, flow, and conservative- and virus-transport observations are considered. The paper examines the use of (1) observed-value weighting, (2) breakthrough-curve temporal moment observations, and (3) the significance of changes in the transport time-step size. The results suggest that (1) sensitivities using observed-value weighting are more susceptible to numerical solution variability, (2) temporal moments of the breakthrough curve are a more robust measure of sensitivity than individual conservative-transport observations, and (3) the transport-simulation time step size is more important than the inactivation rate in solution and about as important as at least two other parameters, reflecting the ease with which results can be influenced by numerical issues. The approach presented allows more accurate evaluation of the information provided by observations for estimation of parameters and generally improves the potential for reasonable parameter-estimation results.

Keywords: Regression analysis; Sensitivity analysis; Solute transport; Viruses; Sorption; Reaction

* Corresponding author. Tel.: +1 303 499 8210.
E-mail address: gilbarth@comcast.net (G. Barth).

0169-7722/$ - see front matter © 2004 Elsevier B.V. All rights reserved.
doi:10.1016/j.jconhyd.2004.10.001

1. Introduction

Using numerical methods to assess the potential for virus contamination of groundwater drinking-water supplies is challenging for many reasons including: (1) virus contamination typically occurs when the rate of transport from the virus source is relatively fast, which reflects advection-dominated flow, (2) viruses remain a health threat at concentrations that typically can be more than eight orders of magnitude less than the source concentration, and (3) accurate parameter values can be difficult to determine. Variability of site conditions suggests that a site-specific assessment of the parameter values controlling virus transport is necessary to produce accurate transport predictions (Bales et al., 1997). Sensitivity analysis can be used to determine the relative importance of each parameter so that characterization efforts focus on reducing uncertainty of the most important parameters, providing the most efficient improvement in prediction accuracy. However, modeling the sorptive–reactive processes characteristic of virus transport under the typically advective-transport conditions and over many orders of magnitude of observed concentrations can be problematic, complicating sensitivity analysis and parameter estimation.

Sensitivity analysis and parameter estimation are already complicated by parameter insensitivity and correlation (Poeter and Hill, 1997), and the potential for introducing a bias through the choice of weighting (Anderman and Hill, 1999). In fact, the considerable potential for misuse and misinterpretation has led to publications focused entirely on developing a systematic approach to guide the calculation and interpretation of parameter sensitivities and estimates (e.g., Hill, 1998). The objective of this paper is to address issues specific to sensitivity analysis and parameter estimation of sorptive–reactive transport, improving the potential for accurate calculation of virus-transport parameter sensitivities and parameter estimates. Although presented in the context of the approach suggested by Hill (1998), the analysis and suggestions presented in this work are broadly applicable to typical field site investigations.

The best method for calculating parameter sensitivities depends on the application. For example, Yeh (1986) notes that the adjoint-state method requires less execution time for situations where the number of parameters is greater than the number of observations while the perturbation method and the more accurate sensitivity-equation method, which are often equivalent in terms of execution time, require less execution time if the number of observations is greater than the number of parameters. The relative execution time of each method can also depend on the simulation. Of the methods mentioned perturbation methods are most versatile because they do not require changes to the code. They can, however, be more susceptible to some types of numerical difficulties. In this work, perturbation methods are used, providing a versatile approach, and the associated numerical difficulties are addressed.

Assessment of potential virus contamination typically includes many observations of several types including heads, flows, and conservative and non-conservative transport observations. The information from the various types of observations aids understanding of the physico-chemical system and the processes controlling virus transport. Previous virus-transport sensitivity analysis has focused on more limited types of observations related to virus transport. For example, Yates (1990) used analytical methods to assess

parameter sensitivity using the maximum virus concentration, C_{max}. From a regulatory perspective C_{max} may be useful, but examining only C_{max} emphasizes parameters controlling the breakthrough curve (BTC) peak and does not provide any information on the parameters controlling the tail of the BTC. Campbell-Rehmann and Welty (1999) provides an assessment by comparing the effect of parameter adjustments on virus BTCs. For reactive transport, Tebes-Stevens and Valocchi (2000) calculated sensitivities for a variety of observation types but analyzed results using a dimensional sensitivity, precluding the possibility of comparing the information contributed from different types of observations. This work uses a set of typical observations collected for assessing the potential for virus contamination of a drinking water supply: observations of head, flow, and conservative and virus transport. This paper uses the methods of Hill (1998) to produce a set of dimensionless scaled sensitivities, assess relative parameter importance and, accounting for observation uncertainty, identify which observations and types of observations provide the most information.

The impact of changes to the transport step size (*TSS*) for simulation of sharp concentration fronts, typical of problematic virus transport situations, is examined in this work. Of concern is that when perturbation methods are used to calculate sensitivities, minor concentration variations associated with sharp fronts are exaggerated by the finite-difference approximation used to calculate sensitivities. This paper introduces the concept of defining the *TSS* as a parameter and using its sensitivity to indicate the significance of other parameters relative to the significance of numerical issues related to *TSS*.

Accounting for virus concentrations over multiple orders of magnitude is required because viral contamination remains a significant health threat down to very low concentrations (Yates, 1990). Under such circumstances, computing accurate sensitivities is problematic and requires addressing a number of issues associated with numerical precision, weighting and observation uncertainty. While assessing the impact of parameter adjustment on BTCs (e.g., Campbell-Rehmann and Welty, 1999), or evaluating a single observation (e.g., Yates, 1990) can provide insight, these methods of assessing impact do not make use of the information from observations over the entire range for which they are significant. This paper examines weighting, in the context of observations significant over many orders of magnitude, to develop and present an approach for weighting virus-transport observations.

The weights on observations reflect observation uncertainty, and often equal or are proportional to one divided by the variance of the observation error (Draper and Smith, 1998; Hill, 1998). Different types of observations, for example hydraulic heads or tracer concentrations, typically have weights of different values. Depending on the observation type, weights may be fixed or variable. Head observations typically have fixed weights because the observations are significant over just a few orders of magnitude. Concentration observations significant over many orders of magnitude require the weight to depend on the concentration (e.g., Barlebo et al., 1998; Wagner and Gorelick, 1986). This work includes both fixed and variable weights and examines issues related to the uncertainty associated with different types of observations, especially for highly advective systems with transport observations that are significant over many orders of magnitude.

For observations that span many orders of magnitude, such as concentrations, weights for sensitivity analysis or parameter estimation are often based on either the observed values (e.g., Gorelick et al., 1983), or the simulated values (e.g., Wagner and Gorelick, 1987). Anderman and Hill (1999) identified a bias when using the observed values for calculating weights. This work examines advantages and disadvantages of using the observed vs. simulated values when calculating weights.

To avoid issues associated with the variability of individual concentration observations other publications have used spatial or temporal moments of observed concentrations. For example, Harvey and Gorelick (1995) used quantiles, representing the proportion of total mass having passed a sampler, as a more robust representation of transport information. This paper uses temporal moments of conservative-transport BTCs to obtain conservative-transport information from the typically sharp-front BTCs and improve the potential for calculating accurate sensitivities.

The intent of this paper is to examine the process of obtaining perturbation-method sensitivities and parameter estimates. Using the standard equations for advective–dispersive–sorptive–reactive transport, this paper demonstrates how sensitivity analysis and parameter estimation for the sorptive–reactive system considered can be successfully accomplished. The simplicity of the system evaluated allows identification of issues associated with the process which could be easily overlooked or incorrectly evaluated in more complex systems. This work focuses on the details of the process, some of the many options involved, and how to improve on the process. Results of applying the process are discussed briefly in this paper, and are presented in detail in Barth and Hill (in review). The process is applicable to a wide range of sorptive–reactive constituents. This work is unique in the range of issues considered including (1) weighting that insures importance of virus-transport observations over many orders of magnitude, (2) use of several types of observations, and (3) assessment of the numerical issues resulting from (1) and (2). The methods used in this work for calculating sensitivities and estimating parameters are versatile and directly applicable to virtually any numerical model.

2. Methods

A brief overview of the methods used to simulate virus transport, conduct sensitivity analysis, and estimate parameter values are provided in this section. The reader is referred to other work for additional information. Included are (1) the equations used to represent virus transport, (2) details of the numerical methods, grids and generation of observations, (3) sensitivity-analysis statistics and weighting, and (4) options for the parameter-estimation methodology.

2.1. Equations

This work considers advection, dispersion, sorption, and reaction as the primary mechanisms affecting virus transport using the following equations. Using these mechanisms, virus transport can be simulated as a sorptive, reactive solute using the advective–dispersive equation (e.g., Corapcioglu and Haridas, 1984; Tim and Mostaghimi,

1991; Schijven et al., 1999), which is also applicable to a wide range of sorptive–reactive solutes.

$$\frac{\partial C}{\partial t} = \underbrace{\frac{\partial}{\partial x_i}\left(D_{ij}\frac{\partial C}{\partial x_j}\right)}_{\text{dispersion}} - \underbrace{\frac{\partial}{\partial x_i}(v_i C)}_{\text{advection}} - \underbrace{\frac{\beta}{\theta}\left(C - \frac{\bar{C}}{K_d}\right)}_{\text{non-equilibrium sorption}} - \underbrace{\lambda 1 C}_{\text{inactivation}} \quad i,j = 1,2,3 \tag{1a}$$

$$\frac{\partial \bar{C}}{\partial t} = \underbrace{\frac{\beta}{\rho_b}\left(C - \frac{\bar{C}}{K_d}\right)}_{\text{non-equilibrium sorption}} - \underbrace{\lambda 2 \bar{C}}_{\text{inactivation}} \tag{1b}$$

$$v_i = -\frac{K}{\theta}\frac{dh}{dx_i} \tag{1c}$$

$$D_l = \alpha_l \upsilon + D^*. \tag{1d}$$

Conceptually, the relationship between the dispersion coefficient, dispersivity, velocity, and molecular diffusion is summarized by Eq. (1d), where the subscript l indicates the curvilinear coordinate direction taken along a flowline (Freeze and Cherry, 1979). A full expansion of the fourth order dispersion coefficient can be found in many subsurface transport texts (e.g., Zheng and Bennett, 2002). The following list defines the terms used in Eqs. (1a)–(1d).

C Concentration in solution [ML^{-3}]
$\bar{C}$ Adsorbed concentration [MM^{-1}]
t Time [T]
x Spatial dimension [L]
D_{ij} Dispersion coefficient [L^2T^{-1}]
v_i Interstitial velocity [LT^{-1}]
θ Porosity
ρ_b Bulk density [ML^{-3}]
β Sorption rate [T^{-1}]
K_d Sorption distribution coefficient [L^3M^{-1}]
$\lambda 1$ Inactivation rate in solution [T^{-1}]
$\lambda 2$ Adsorbed inactivation rate [T^{-1}]
K Hydraulic conductivity [LT^{-1}]
α_l Dispersivity [L]
h Hydraulic head [L]
D^* Molecular diffusion [L^2T^{-1}]

From the above list, this paper evaluates the sensitivity of seven parameters (K, θ, α_l, β, K_d, $\lambda 1$, $\lambda 2$) that control transport for a given set of boundary conditions. In the advection-

dominated systems examined in this work D^* does not typically have a significant impact, and ρ_b is typically obtained from independent measurements.

2.2. Numerical simulation

Sorptive–reactive transport is simulated using double precision versions of the groundwater flow program MODFLOW96 (Harbaugh and McDonald, 1996) and the multi-species, sorptive–reactive capabilities of MT3DMS (Zheng, 1998). Double precision is necessary to reduce the effects of round-off error on the sensitivity-analysis and regression results (Poeter and Hill, 1998).

MODFLOW's PCG2 solver (Hill, 1990) was used to solve for heads and flows. As is common for advection-dominated systems, the flow-model solver convergence criteria significantly affected the calculated concentrations and therefore the associated sensitivities. Setting these convergence criteria on the same order as the number of significant digits used in the numerical solution resolves this issue.

MT3DMS uses operator splitting so that the advective term is calculated separately from the other terms. The Total Variation Diminishing (TVD) method was used to solve the advection term, and the standard explicit method was used to solve the other terms. The implicit method was not used because this investigation targets simulations that include sharp fronts. The very small time-step size necessary for the implicit solver to represent accurately the sharp front eliminated its potential advantages.

2.2.1. One- and two-dimensional grids

In this work, perturbation-based methods of sensitivity analysis and parameter estimation are performed using simulations of one- and two-dimensional systems. The one-dimensional system is used to identify numerical-solution issues. The two-dimensional system is used to demonstrate the precautions needed to insure accurate sensitivities and parameter estimates when simulating flow and transport in multi-dimensional systems, and to examine longitudinal spatial trends in sensitivities.

The one-dimensional grid consists of 160 finite-difference cells, each 0.0635 m long. The overall transport distance is 10.16 m. Constant-head boundaries are imposed. The flow system is steady state. An initial concentration, representing a finite duration injection pulse immediately after injection, is located at the upgradient boundary.

The two-dimensional grid consists of 40 rows and 160 columns. Constant-head boundaries are imposed at each end, and no-flow boundaries along the length of the system. Each finite-difference grid cell measures 0.0254 by 0.0635 m, producing a domain just over 1 m tall and 10.16 m long (Fig. 1). The source is centered along the upgradient boundary, spanning 0.254 m.

2.2.2. Generating hydraulic head, flow and concentration observations

To insure a controlled situation in which sensitivity analysis and parameter estimation can be evaluated most clearly, observed quantities are generated using the constructed one- and two-dimensional models. For the 1D grid, head, conservative-solute, and virus observations are from eight locations. The longitudinal distances are the same as for the two-dimensional grid shown in Fig. 1. For both the 1D and 2D grids, bulk flow through

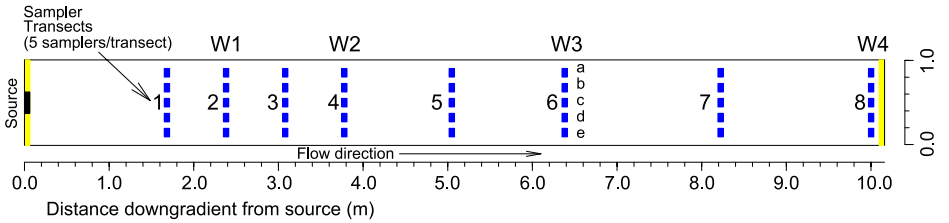

Fig. 1. Two-dimensional finite-difference domain, source, and observation locations. Labels above even-numbered sampler transects correspond to wells sampled by Schijven et al. (1999).

the system is used as the single flow observation. In the 2D grid, each of the eight sampling transects provide head and transport observations at five locations. Individual transport observations are comprised of the flux-averaged concentration from four finite-difference cells. Symmetry of the sampler layout about the longitudinal centerline helped identify numerical artifacts that are often manifested as asymmetric simulated values and sensitivities.

Parameter values in Table 1 are the average values from virus transport field experiments (Schijven et al., 1999) and were used in the forward runs to produce noiseless observations of heads, flows, and conservative and virus concentrations. The field experiments consisted of introducing viruses and a conservative solute into a dune recharge system in Castricum, the Netherlands. They determined the parameter values by fitting observations with a one-dimensional model and by direct measurement.

For most simulations, noise is added to the simulated values to create the observations. For flows and heads noise is added as:

$$y_{i,j}^{k} = \hat{y}_{i}^{k} + \sigma_k R_{i,j}^{k} \tag{2}$$

where $\hat{y}_i^k$ is the simulated value, $\hat{y}_{i,j}^{\ k}$ is the 'observed' value, k indicates the observation type (flow $k=f$, or head $k=h$), i is the observation number, σ_k is the standard deviation of typical measurement error and, in this study, is the same for all observations of type k. For this work the standard deviation of typical measurement error for heads and flows was

Table 1
Parameter values

Parameter	Value
K, hydraulic conductivity (m day^{-1})	12[a]
α, dispersivity (m)	0.032[a]
θ, porosity	0.35[a]
K_d, sorption distribution coefficient (m^3 kg^{-1})	0.238[a]
β, sorption rate (day^{-1})	0.747[a]
$\lambda 1$, inactivation in solution (day^{-1})	0.075[b]
$\lambda 2$, inactivation adsorbed (day^{-1})	0.07[a]
TSS, transport step size (day)	0.01

[a] Estimated by Schijven et al. (1999).
[b] Measured by Schijven et al. (1999).

calculated based on coefficients of variation of 0.001 and 0.005, respectively, reflecting this investigation's emphasis on the development of a process for calculating sensitivities and parameter estimates. A process that would typically be less challenging to perform consistently and accurately in the presence of increased noise, which would tend to decrease the range over which concentration observations remained significant. As discussed in the section on weighting, the weights associated with these fairly small measurement errors can be quite large, and requires a well-developed approach to generating sensitivities and parameter estimates. The value used for R_{ij} is the jth set of standard-normal random noise (James, 1994) generated for the ith observation. Eq. (2) uses a fixed level of noise. The noise does not depend on the magnitude of the observation, reflecting the fact that in this work observations such as heads and flows have a limited range of variation.

Concentrations significant over many orders of magnitude require that noise added to the concentrations is variable, proportional to the magnitude of the simulated value:

$$y^{c}_{i,j} = \hat{y}^{c}_{i}\left(1 + \mathrm{Cv}_i R^{c}_{i,j}\right) \tag{3}$$

where the superscript c identifies concentration observations, and Cv_i is the coefficient of variation for the ith observation. The coefficient of variation used for concentrations was 0.08. To avoid numerical and computational issues associated with zero-concentration observations and their weighting, a detection limit equal to the concentration at which viruses were no longer considered a health threat was included in the simulations; a normalized concentration value of 10^{-8} was used, with concentrations normalized to the initial concentration. Fig. 2 shows an example of observations before and after adding

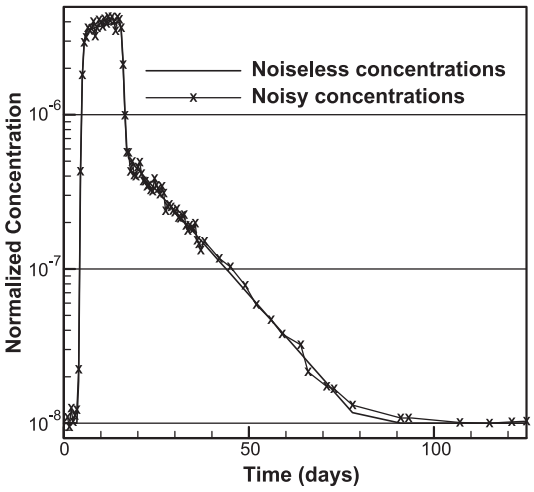

Fig. 2. Generated concentration observations. Noise was added to simulated concentrations to create concentration observations. The variance of the noise increased with concentration. Data shown is from Transect 6, sampler c, the middle sampler.

noise, and effect of the detection limit. For a noiseless realization j=0 and R_{ij}=0.0, so that no noise is added. Noiseless realizations were used to detect numerical-solution issues that could be obscured by the presence of noise.

2.2.3. Representing transport observations using temporal moments

Temporal moments of conservative-transport BTCs are used as an alternative form of representing conservative-transport observations for two reasons. First, sensitivities calculated for temporal moments are less susceptible to minor asymmetries and variability associated with numerical errors that occur for conservative transport in highly advective systems. Second, the BTC moments remain sensitive even when the predicted conservative-transport BTC does not overlap the observed BTC, in which case, as discussed in the results, the scaled sensitivities of individual concentration observations are insignificant. This occurs because, in contrast to individual conservative-transport observations, the objective-function contribution from temporal-moment weighted residuals increases monotonically as the simulated BTC moves farther from the observed, regardless of the separation between simulated and observed BTCs.

This paper uses the normalized first moment (m_1),

$$m_1 = \frac{M_1}{M_0} \quad \text{where } M_j = \int_0^\infty t^j y^c(x,t)\mathrm{d}t \text{ and } j = 0, 1 \tag{4}$$

where t^j is time raised to the power j, and $y^c(x, t)$ is concentration as a function of space and time. The term m_1 provides a lumped indicator of the mean arrival time. Noise is not directly generated for moments, but is present due to the noise in the $y^c(x, t)$ values. In this work the resulting variance of error in the moments is considered to be fixed: it is independent of the value of the moment.

2.2.4. Individual concentration observations vs. temporal moments

In calculating m_1, individual observations are not weighted, so the moments primarily reflect the higher concentration conservative-transport observations. In this work, low concentration conservative-transport observations do not contribute significantly in terms of characterizing flow and transport. Therefore, the moments of conservative-transport observations provide sufficient information for sensitivity analysis and parameter estimation. In systems with a more dispersed or a multiple-peaked conservative transport BTC, it may be beneficial to retain individual conservative-transport observations, or may warrant a combination of the individual observations and moments.

Concentration observations of virus transport are used and weighted individually to provide feedback over many orders of magnitude. The lower virus concentrations provide significant information regarding reactive and sorptive transport parameters and the long BTC tails tend to insure at least some overlap between the observed and simulated values. The section on weighting discusses additional motivation for using conservative- but not virus-transport BTC temporal moments. Examples demonstrating the issues encountered calculating sensitivities using individual conservative-transport observations are summarized in Section 3.

2.2.5. Transport step size issues

Perturbation sensitivity methods allow complete flexibility so that any model input can be treated as a parameter. In this work *TSS* is one of the parameters evaluated for its potential to affect sensitivity analysis and parameter estimation results, and serve as an indicator of the level below which other parameters will have limited significance for the system simulated.

In most numerical transport simulators, including MT3DMS, the simulation-time discretization, or *TSS*, is adjusted to balance stability, accuracy, and execution time constraints. For advection alone adjusting *TSS* to keep the Courant Number ($Cr=v\Delta t/\Delta x$) less than 1.0 is usually sufficient to produce a stable solution with minimal numerical dispersion. Transport with sorption and inactivation requires additional constraints to insure that operator splitting mass-balance errors remain small (Kinzelbach et al., 1991; Valocchi and Malmstead, 1992). For multiple solute species, including a species experiencing non-equilibrium sorption and first-order irreversible reaction, MT3DMS determines the largest value of *TSS* small enough to satisfy the constraints of all of the components, TSS_0, calculated as (Zheng, 2000):

$$TSS_0 \leq \frac{1}{\frac{1}{\Delta t_{\mathrm{ADV}}} + \frac{1}{\Delta t_{\mathrm{DSP}}} + \frac{1}{\Delta t_{\mathrm{SSM}}} + \frac{1}{\Delta t_{\mathrm{RCT}}}} \tag{5a}$$

Δt_{ADV}, Δt_{DSP}, Δt_{SSM}, and Δt_{RCT} are defined as:

$$\Delta t_{\mathrm{ADV}} \leq \frac{Cr}{\left(\frac{|v_x|}{\Delta x} + \frac{|v_y|}{\Delta y} + \frac{|v_z|}{\Delta z}\right)} \tag{5b}$$

$$\Delta t_{\mathrm{DSP}} \leq \frac{0.5}{\left(\frac{D_{xx}}{\Delta x^2} + \frac{D_{yy}}{\Delta y^2} + \frac{D_{zz}}{\Delta z^2}\right)} \tag{5c}$$

$$\Delta t_{\mathrm{SSM}} \leq \frac{\theta}{q_{\mathrm{s}}} \tag{5d}$$

$$\Delta t_{\mathrm{RCT}} \leq \frac{1}{\lambda 1 + \lambda 2} \tag{5e}$$

where v_x, v_y, v_z, D_{xx}, D_{yy}, D_{zz}, Δx, Δy, Δz are the velocity, dispersion coefficients, and numerical grid-cell size in the x, y, and z coordinate directions, respectively, and q_{s} is the sink or source volumetric flow rate per unit volume of aquifer. Changes in parameter values K, θ, α_l, $\lambda 1$, or $\lambda 2$ may cause a change in TSS_0, resulting in minor changes to simulated transport but significant changes in sensitivities. Regression runs, where parameters may be updated to values significantly different than their starting values, or sensitivities calculated using perturbation methods (e.g., Poeter and Hill, 1998) can be adversely affected. As shown below, the problem becomes more severe for simulations

with high Peclet numbers ($Pe=\Delta x/\alpha_l>2$) because simulated concentrations may change dramatically along sharp fronts for small changes in *TSS*.

2.3. Sensitivity analysis

Sensitivity analysis is used here to identify the information observations contain for estimating parameters, insensitive and correlated parameters that are likely to cause the regression to perform poorly, and to diagnose difficulties and limitations of the parameter-estimation results (Hill, 1998).

2.3.1. Calculation of sensitivities

Sensitivities were calculated using UCODE (Poeter and Hill, 1998). Centered-difference sensitivities were used and are calculated as,

$$\frac{\partial \hat{y}_i}{\partial b_j} \approx \frac{\hat{y}_i\left(\underline{b}+\Delta \underline{b}_j\right)-\hat{y}_i\left(\underline{b}-\Delta \underline{b}_j\right)}{2\Delta \underline{b}_j} \tag{6}$$

where b_j is the jth parameter, $\Delta \underline{b}_j$ is a vector with one nonzero term, and the subscript j indicates the jth component in $\Delta \underline{b}_j$ equals Δb_j, the amount that the jth parameter value is perturbed. It is possible to calculate an optimal perturbation size (e.g., Dennis and Schnabel, 1996, p. 99), but this investigation uses a perturbation size fixed at 1% of the parameter value, as suggested in the UCODE documentation (Poeter and Hill, 1998, p. 33). Trial and error evaluation of perturbation-size impact confirmed that a 1% perturbation size was appropriate for this investigation.

2.3.2. Statistics of the sensitivity analysis

In this work, $\hat{y}_i$ and $\underline{b}_j$ can represent a range of observations and parameters of different types and units. As a result, the sensitivity values calculated using Eq. (6) in general are not directly comparable. To determine how much information the observations provide towards estimating the different parameters, scaled sensitivity measures are used, including dimensionless scaled sensitivities (dss) and composite scaled sensitivities (css) (Hill, 1998).

For a diagonal weight matrix ($\underline{\omega}$), the dimensionless scaled sensitivities for observation $\hat{y}_i$ and parameter b_j are calculated as,

$$\mathrm{dss}_{ij} = \left(\frac{\partial \hat{y}_i}{\partial b_j}\right) b_j \omega_i^{1/2} \tag{7}$$

where $\omega_i^{1/2}$ is the square root of the weight of observation $\hat{y}_i$, and in this work equals one divided by the estimated standard deviation of the observation errors, as discussed below. Dimensionless scaled sensitivities are used to evaluate the importance of individual observations in the estimation of each parameter. The scaling provided by b_j and $\omega_i^{1/2}$ allows comparison of sensitivities despite different units and observation uncertainty.

Composite scaled sensitivities (css) are calculated for each parameter as,

$$\mathrm{css}_j = \left[\frac{\sum_{i=1}^{\mathrm{ND}} \left(\mathrm{dss}_{ij}\right)^2 \Big|_{\underline{b}}}{\mathrm{ND}} \right]^{1/2} \tag{8}$$

where ND is the number of observations and can include all head, flow, conservative-tracer, and virus transport observations, or a subset that could be based on observation type, location, and/or timing. The value of css_j indicates the total information provided by the ND observations for the estimation of the jth parameter.

For this work, css values are calculated for concentrations from each sampler or transect of samplers. In the one-dimensional system temporal moments of conservative transport BTCs and virus BTCs, from each location, are composited with the one system flow observation to produce css's for each sampling location. In the two-dimensional system, conservative transport first temporal moments and virus BTCs from the samplers in each of the eight transects are composited with the one flow observation and head observations from the entire system, resulting in eight css values for each parameter. This compositing is similar to what would be done for a site investigation, allowing assessment of spatial trends in transport-observation importance, and reflects typical field-site investigation circumstances: an abundance of head observations and a relatively limited number of flow observations and concentration-observation locations.

The sensitivity of the simulation results to the value of *TSS* can be determined by treating *TSS* as a parameter. Sensitivities are calculated as

$$\frac{\partial \hat{y}_i}{\partial TSS} \approx \frac{\hat{y}_i\left(\underline{b} + \Delta \underline{b}_{TSS}\right) - \hat{y}_i\left(\underline{b} - \Delta \underline{b}_{TSS}\right)}{2\Delta \underline{b}_{TSS}} \tag{9}$$

where $\Delta \underline{b}_{TSS}$ is a vector with one nonzero term, which equals Δb_{TSS}, the amount that *TSS* is perturbed.

2.3.3. Weighting issues and approaches

For a valid regression weights need to be proportional to one divided by the variance of the observation error (σ_i^2) (Draper and Smith, 1998, p. 222). In this work, as suggested by Hill (1998), an equality is used so that

$$\omega_{k_i} = \frac{1}{\sigma_{k_i}^2} \quad \text{where } i = 1 \ldots ND. \tag{10}$$

In this work, the value $\sigma_{k_i}^2$ is known because the observations are synthetic, created with known error variances and there is no model error to consider (Hill and Tiedeman, 2003). Hill (1998) discusses methods for estimating $\sigma_{k_i}^2$ for real data sets. For each observation of head ($k=h$), flow ($k=f$), and temporal moments of the conservative-transport BTCs ($k=m$) a fixed weight is used because, in this work, the observations vary and are significant over a limited range.

Conservative- and virus-transport concentrations use a variable weight because $\sigma^2_{c_i}$ is proportional to the concentration. Weights ideally would be calculated using the true concentration values, that is,

$$\omega_{c_i} = \frac{1}{\left(\mathrm{Cv}_i \tilde{y}_i^{\mathrm{c}}\right)^2} \quad \text{where } i = 1\ldots\mathrm{nc} \tag{11}$$

where nc is the number of observations with weights proportional to their value, Cv_i is the coefficient of variation, and $\tilde{y}_i^{\mathrm{c}}$ is the true concentration. Incorporation of a detection limit avoids very small concentrations and the result that Eq. (11) would become excessively large. The value of $\tilde{y}_i^{\mathrm{c}}$ is, in general, unknown and is approximated using either the observed (e.g., Keider and Rosbjerg, 1991) or simulated value (e.g., Wagner and Gorelick, 1986). Anderman and Hill (1999) compare the two approaches.

In an alternative, equivalent method the concentration residual is scaled by the observed or simulated concentration and weights are equal to $1/\mathrm{Cv}_i^2$ (Van Rooy et al., 1989; Barlebo et al., 1998). Van Rooy et al. (1989) and Barlebo et al. (1998) also include a parameter estimation scaling factor, discussed below, in the objective function that changes the relative weighting of groups of observations.

2.4. Parameter estimation

Parameters are estimated by quantifying the fit between observed and simulated values and minimizing with respect to the parameter values. Here, a weighted least-squares objective function, $S(\underline{b})$, quantifies the fit as:

$$S\left(\underline{b}_r\right) = \left[\underline{y} - \underline{\hat{y}}\left(\underline{b}_r\right)\right]^T \underline{\omega} \left[\underline{y} - \underline{\hat{y}}\left(\underline{b}_r\right)\right]. \tag{12}$$

The weight matrix, $\underline{\omega}$, and observed- and simulated-value vectors, $\underline{y}$ and $\underline{\hat{y}}(\underline{b})$, respectively, include terms for all the observations, and the subscript r indicates the parameter estimation iteration number. The objective function is minimized using a modified Gauss–Newton method (e.g., Seber and Wild, 1989; Sun, 1994) as described in Hill (1998).

Several investigations (e.g., Barlebo et al., 1998; Keider and Rosbjerg, 1991; Van Rooy et al., 1989; Carrera and Neuman, 1986) use a scaling factor in an approach referred to by Bard (1974, p. 62) as stagewise optimization to adjust the relative importance of different observation types. In this work, using UCODE (Poeter and Hill, 1998), the objective function is divided into two components,

$$S_k\left(\underline{b}_r\right) = \sum_{i=1}^{\mathrm{nk}} \omega_{k_i} \left(y_{k_i} - \hat{y}_{k_i}\left(\underline{b}_r\right)\right)^2 \tag{13}$$

and

$$S_c\left(\underline{b}_r\right) = \sum_{j=1}^{\mathrm{nc}} \omega_{c_j} \left(y_{c_j} - \hat{y}_{c_j}\left(\underline{b}_r\right)\right)^2 \tag{14}$$

where nk and nc are the number of observations with fixed weights (in this work, heads, flows and moments) and variable weights (in this work, concentrations), respectively, and $S_k(\underline{b}_r)$ and $S_c(\underline{b}_r)$ represent the fixed- and variable-weight components, respectively, of the objective function,

$$S(\underline{b}_r) = S_k(\underline{b}_r) + S_c(\underline{b}_r). \tag{15}$$

The ratio of relative contributions is used as the basis for a scaling factor χ,

$$\chi_{r-1} = \frac{\dfrac{S_k(\underline{b}_{r-1})}{\mathrm{nk}}}{\dfrac{S_c(\underline{b}_{r-1})}{\mathrm{nc}}} \tag{16}$$

where $r-1$ indicates the use of values from the previous iteration. The values of ω_{k_i} are as indicated in Eq. (10), ω_{c_j} is determined at each iteration as:

$$\omega_{c_j} = \frac{\chi_{r-1}}{\left(\mathrm{Cv}_j \hat{y}_{c_j}\right)^2} \tag{17}$$

which, substituted into Eq. (14) results in,

$$S_c(\underline{b}_r) = \sum_{j=1}^{\mathrm{nc}} \frac{\chi_{r-1}}{\left(\mathrm{Cv}_j \hat{y}_{c_j}\right)^2} \left(y_{c_j} - \hat{y}_{c_j}(\underline{b}_r)\right)^2 \tag{18}$$

reflecting the dependence of the current-iteration objection function value on the results of the previous iteration.

The objective-function scaling parameter, χ_{r-1}, adjusts the contributions to the objective function so that the average contribution of $S_k(\underline{b}_r)$ is comparable to the average contribution of $S_c(\underline{b}_r)$. This adjustment is intended to improve the regression's potential to estimate parameters based on the information from all observations, reducing the chance that one group of observations will dominate the value of the objective function. While serving a practical role during the regression, it is important to consider the following two issues. First, the value of χ_{r-1} changes with successive iterations. Oscillations in χ_{r-1} can cause large changes in weighting and the objective function surface at each iteration of the parameter estimation, reducing the potential for convergence and/or accurate parameter estimation. Second, if at the final iteration χ_{r-1} is significantly different than 1.0 it may produce weights that are not proportional to the inverse of the variance of the measurement error, which is necessary for a valid regression and reflected in the original weighting. In such a case a final step may be necessary, revaluating the system using the estimated parameter values and setting χ_{r-1}=1.0.

3. Results and discussion

This section focuses on six results of the simulations conducted: (1) selection of temporal moments instead of individual conservative-transport observations, (2) *TSS*

sensitivity, (3) how well the scaled sensitivities reflect observation importance, (4) considerations for residual weighting, (5) effects of the scaling factor in the parameter-estimation objective function, and (6) a summary of sensitivity analysis and parameter estimation results.

3.1. Issues associated with using individual conservative-transport observations

Preliminary sensitivity runs, not presented in this work, revealed errors in css values calculated for conservative concentrations: css values were not equal, but should have been, for samplers that were symmetrically positioned about the longitudinal center line of the system. To demonstrate, consider sampler transect 6 in Fig. 1. Sampler b, above the longitudinal center line, should have the same calculated css as sampler d, which is an equal distance below the center line. However, preliminary sensitivity runs produced a sampler b css 20% larger than the sampler d css. There are two primary reasons for this inconsistency, both of which suggest problems with using individual concentration observations.

First, even for the simple conditions evaluated, the flow-field solution error was sufficient to produce a slightly non-symmetric solute plume. With a head convergence criterion of 10^{-5}, a 0.41% difference in concentration between samplers b and d was not unusual. Error in the calculated concentrations, especially lower concentrations which typically have greater weights when using weights based on simulated concentrations, produced sensitivities that were asymmetric: a 20% difference in calculated sensitivity between samplers b and d was not unusual. It was also evident that the two sets of calculations, (1) transport based on the flow field, and (2) parameter sensitivities based on transport, tended to increase the significance of the asymmetry by orders of magnitude. A flow-field solution error of 0.001% resulted in samplers b and d having concentration differences of about 0.4% and dss_K differing by about 10%. As a result, minor flow field errors caused css values, that should have been identical, to differ by up to 23%. Decreasing the convergence criteria to 10^{-13}, so that the flow-model error was on the same order as the precision of the numerical calculations, eliminated this source of error for the system simulated, but may not be a viable option for more complex systems.

Second, often a single observation, and therefore a single dss, effectively determines the css for an entire BTC. Focusing on advection dominated systems and using weights to insure significance over many orders of magnitude produces a combination of rapid concentration transitions and a large range of weights. Under these circumstances the accuracy achievable using perturbation-method sensitivity calculations results in the css being susceptible to situations where a few observations at the base of a sharp-front BTC rising limb exhibit relatively large changes as parameters are perturbed, and the change is given considerable weight due to the low initial concentration. For example, in a typical preliminary sensitivity-analysis evaluation of a conservative transport BTC, 75% of the css magnitude was from just two of the 70 observations.

Replacing or augmenting individual concentration measurements with m_1 eliminates both of the issues discussed. As a lumped statistic m_1 is far less susceptible to numerical issues that might adversely permit a few observations to dominate the contribution of the entire BTC. Being a measure of mean arrival time, m_1 is not significant over multiple

orders of magnitude, reflecting that the low-concentration conservative-transport observations are not critical for this evaluation and that there is no need to create weights ranging over multiple orders of magnitude. In addition to the previously discussed benefit of remaining sensitive even when the predicted conservative-transport BTC does not overlap the observed BTC, using m_1 in place of individual concentration measurements produced a set of sensitivity results that were symmetric about the longitudinal axis and provided a set of calculated sensitivities that did not exhibit numerically induced variability.

It is possible that for different circumstances the choice between BTC temporal moments and individual concentration observations may not be as straightforward. Examples include a more dispersive system, heterogeneity that produces multiple-peak conservative-transport BTCs, or an extremely sparse observation data set. Considering the benefits of temporal moments, the approach would be worth evaluating for most situations. Whether to use 1st moments only, combining them with individual concentration observations, and(or) using 2nd order temporal moments to reflect BTC spreading (Shapiro and Cvetkovic, 1988; Barth et al., 2003) is problem dependent.

3.2. Transport step-size (TSS) sensitivity

This work demonstrates the sensitivity of transport simulation results to *TSS*, and that *TSS* sensitivity can surpass some of the less sensitive virus-transport parameters. For example, a 1% perturbation of $\lambda 1$, a parameter that does not affect conservative transport, may change TSS_0, resulting in a nonzero sensitivity of conservative transport observations to $\lambda 1$. This issue can be addressed by fixing *TSS* at a sufficiently small value. In this work, *TSS* is fixed at TSS_f such that $TSS_f \sim (0.8)TSS_0$, where TSS_0 is calculated by MT3DMS, using initial parameter values in Eqs. (5a)–(5e). Setting $TSS_f=(0.8)TSS_0$ is a compromise to keep execution time as short as possible without having significant mass-balance errors and avoiding the possibility of simulation-result changes due to changes in *TSS*. Parameter value changes that force $TSS<TSS_f$ requires repeating the parameter estimation with a smaller value of TSS_f if sensitivity to css_{TSS} is comparable to css of other parameters.

Fixing the $TSS<TSS_0$ means that the Courant number, *Cr*, may be different for each forward run used to calculate the perturbation sensitivities. The potential differences in simulated transport observations would be largest for advective systems where the physical dispersion is small. However, for this work a fixed *TSS* is used because (1) a primary objective is generating accurate sensitivities, (2) the impact due to *Cr* differences is minor, and (3) the resulting variations in *Cr* are small compared to what can be expected for a heterogeneous system where *Cr* will vary throughout the domain since a single value *TSS* must be used for the entire model domain. This reasoning also suggests the use of a fixed *TSS* for many other systems.

If css_{TSS} is larger than css of one or more of the other parameters, sensitivity analysis and estimation of those parameters may be susceptible to variability in *TSS*. In this work, for the set of parameters evaluated, $css_{TSS}>css_{\lambda 1}$ (Fig. 3) suggesting that changes in *TSS* affect simulated results more than changes in the in-solution inactivation parameter, $\lambda 1$. Different parameter values may produce situations where $css_{TSS}<css_{\lambda 1}$ or where css_{TSS} is larger than the css of a different parameter. Obtaining $css_{\lambda 1}$, for the conditions simulated,

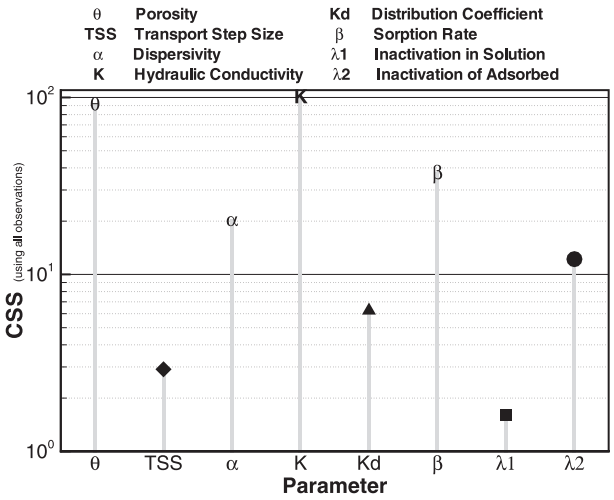

Fig. 3. Composite-scaled sensitivities of the seven parameters and *TSS*. Composite scaled sensitivities indicate the parameters that are most important for reproducing the observed values. K and θ are the most important parameters, *TSS* is more important than the rate of inactivation in solution ($\lambda 1$).

required fixing $TSS \sim 0.8 TSS_0$. In general, this precaution is necessary for applications that include less sensitive parameters: if *TSS* is not fixed, the amount of information provided by the parameter cannot be calculated accurately, which will affect parameter estimation regardless of the parameter estimation method.

3.3. Issues and precautions for calculating sensitivities

The ability of dimensionless and composite scaled sensitivities to reflect the information contained in observations is influenced by both the calculated unscaled sensitivity and the scaling used in the weights.

Unscaled sensitivities can vary for reasons such as numerical solution variability in advection-dominated systems. For example, in transport simulations, a value of $Pe > 2.0$ can produce small variations in simulated transport that can have a dramatic impact on calculated derivatives. Fig. 4 uses examples from a one-dimensional simulation with a sharp concentration front to illustrate the issue. Composite-scaled sensitivities of hydraulic conductivity are calculated for each of the eight observation locations using the flow observation, conservative-transport moments, and virus-transport observations from each sampling transect. Fig. 4 shows the trend with distance from the source for grid refinements of 80, 160, 640 and 2560 nodes, corresponding to $Pe = 16$, 8, 2, and 0.5, respectively. Transport through more dispersive systems will tend to reduce the potential for a sharp front and associated variability of the numerical solution. However, virus transport must often be characterized for highly advective systems over distances on the order of tens of meters where there is limited opportunity for smoothing of a sharp concentration front. Finally, it is worth considering heterogeneous systems and the effect

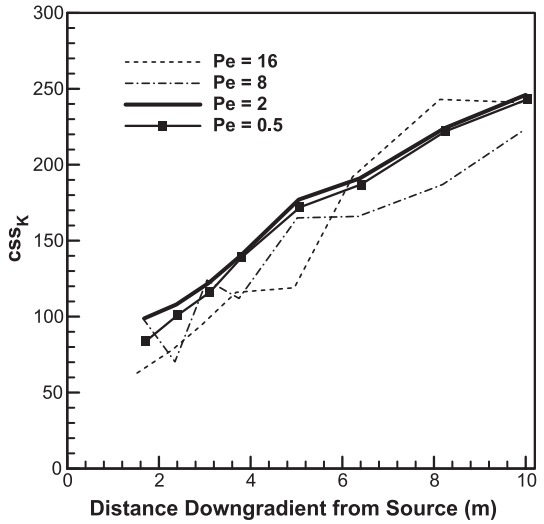

Fig. 4. Hydraulic conductivity composite scaled sensitivity, css_K, calculated for observation locations at different distances from the source for four grid refinements corresponding to grid Peclet numbers ranging from 0.5 to 16, reflecting grid refinements that range from 2560 to 80 nodes, respectively. The erratic css_K values for grid Peclet numbers>2 suggest numerical difficulties are corrupting the perturbation sensitivities and that parameter estimates will probably be affected.

of the local *Pe* in heterogeneous systems. These results suggest that, at locations where the local value of *Pe* exceeds 2.0, the calculated sensitivity of a spatially varying parameter may reflect a combination of parameter importance and numerical variability at that location.

Of special concern in the scaling used is that the weights determined using Eq. (11) range widely because virus concentrations are significant over eight orders of magnitude. This can exacerbate any variations in the unscaled sensitivity. Problems occur for both observed and simulated-value weighting, OVW and SVW, respectively, but differ in their effect. Benefits and drawbacks of using OVW and SVW for calculating sensitivities were examined and are summarized in Table 2. SVW has two primary advantages: (1) it produces scaled sensitivities that better reflect parameter importance for the simulated transport, especially as simulated values become considerably different from observed, and (2) it results in unbiased weighted residuals (Anderman and Hill, 1999). OVW can distort the dss resulting in just a few observations dominating the css of a parameter: significant unscaled sensitivities in conjunction with large weights based on small observed values produce a few large dss that predominately determine the updating of the parameter vector during the regression. Fig. 5 demonstrates this issue using observed and simulated conservative-transport BTCs, unscaled sensitivities, and OVW- and SVW-scaled sensitivities. The simulations were performed using an unoptimized set of parameter values. The unscaled and SVW-scaled sensitivities reflect the shape of the simulated BTC: the largest sensitivities correspond to the portions of the BTC that change most for a change in *K*. In contrast, the values of the OVW-scaled sensitivities are

Table 2
Alternative transport weighting approaches

Weighting approach	Equivalent forms[a]	Issues		
		Sensitivity (Fig. 5)	Weighted residual (Figs. 6, 7 and 8)	Parameter estimates
OVW[b]	$\frac{y_i^c - \hat{y}_i^c}{y_I^c}\left(\frac{1}{\mathrm{Cv}_i}\right)$	dss for observations where $\hat{y}_i^c > y_i^c$ can be much larger than all other dss	Negative transport-observation weighted residuals[c] can be much larger than all others	Biased
SVW[d]	$\frac{y_i^c - \hat{y}_i^c}{\hat{y}_i^c}\left(\frac{1}{\mathrm{Cv}_i}\right)$		Positive transport-observation weighted residuals[c] can be much larger than all others	Unbiased

[a] In the equivalent forms, residuals are normalized with observed or simulated values and the weights are based on the coefficient of variation.
[b] OVW: Observed-value weighting: weights in Eq. (11) are calculated using observations.
[c] Residuals are calculated as observed minus simulated concentrations ($y_i^c - \hat{y}_i^c$).
[d] SVW: Simulated-value weighting: weights in Eq. (11) are calculated using simulated concentrations.

dominated by the combination of large weights (due to small observed values) with large unscaled sensitivities. In Fig. 5, only a few of the observations with large unscaled sensitivities have significant values of OVW-scaled sensitivities. The SVW-scaled sen-

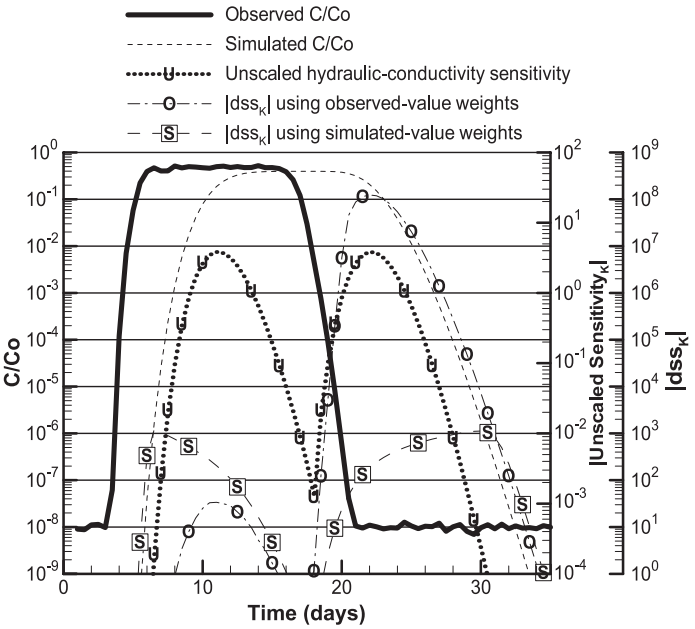

Fig. 5. Observed and simulated breakthrough curves with hydraulic-conductivity (K) dimensionless-scaled sensitivities (dss$_K$) using observed- and simulated-value weighting. The dss$_K$ produced using observed-value weighting are extremely large when large unscaled sensitivities coincide with large weights resulting from small observed values. Simulated-value weighting produces dss$_K$ that more realistically reflect the importance of hydraulic conductivity on the simulation and reduce the potential for unstable parameter-estimation runs.

sitivities will provide much better insight as to the observations that contain information, while the OVW-scaled sensitivities can be misleading since only a limited portion of the observations, associated with small observed values, are the most influential. The limited number and magnitude of the OVW-scaled sensitivities also result in a set of sensitivities far more susceptible to small variations in the numerical solution. In contrast, SVW cannot result in a combination of significant unscaled sensitivities and large weights associated with small concentrations. The SVW-scaled sensitivities are a better representation of the impact of changes in K on the simulated concentrations. This comparison between OVW and SVW scaled sensitivities is not to advocate creating scaled sensitivities with the exact same emphasis as the unscaled sensitivities, this would defeat one of the major incentives for scaling. The comparison demonstrates that SVW-scaled sensitivities more accurately reflect the observation information and that OVW-scaled sensitivities can be dominated by a few observations that, in general, should not be emphasized over other observations.

3.4. Residual-weighting issues

As with sensitivity analysis, the combination of typical virus-transport conditions and the significance of concentration over a wide range can make parameter estimation susceptible to numerical issues. These issues include (1) residuals in the flow field, (2) oscillations in the transport solution, and (3) sharp fronts.

The weighted residual on the ith concentration observation (e_i^c) is defined as

$$e_i^c = \left(y_i^c - \hat{y}_i^c\right)\omega_{c_i}^{1/2} = \left(y_i^c - \hat{y}_i^c\right)\frac{1}{\mathrm{Cv}_i\tilde{y}_i^c}. \tag{19}$$

For values of normalized concentration ranging from 0 to 1.0, when either the simulated or observed value is considerably larger than the other, the absolute value of the residual approaches 1.0 and the absolute value of the weighted residual approaches

$$\left|e_i^c\right| \approx \omega_{c_i}^{1/2} = \frac{1}{\mathrm{Cv}_i\tilde{y}_i^c}. \tag{20}$$

For concentrations that are significant over eight orders of magnitude, there would typically be a difference of more than seven orders of magnitude for positive vs. negative weighted residuals. Fig. 6 demonstrates that, for observations that are significant over so many orders of magnitude, both OVW weighted residuals (e_{ovw}) and SVW weighted residuals (e_{svw}) have the potential to be very large. The size of these weighted residuals means that any error in the sensitivity resulting from numerical difficulties has greater potential to prevent successful convergence. This can be especially problematic when insensitive parameters are involved or when there are only a limited number of transport observations.

In contrast to scaled-sensitivity calculations, e_{svw} offer a more subtle advantage that is best demonstrated using a set of examples. When using OVW, weighted residuals are largest for negative residuals (simulated values greater than the observed), while SVW produces weighted residuals that are largest for positive residuals.

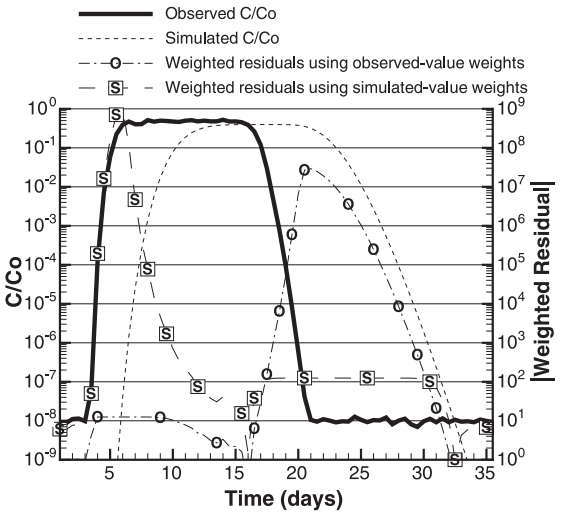

Fig. 6. Simulated breakthrough curve trailing but overlapping the observed breakthrough curve, and weighted residuals using observed- and simulated-value weighting. Observed-value weighted residuals are very large when large residuals combine with large weights, resulting from small observed values. Analogously simulated weighted residuals are very large when large residuals coincide with small simulated values. In both cases there is potential for a few weighted residuals to dominate the objective function, making the system more susceptible to numerical variability.

Three scenarios are considered to illustrate similarities and differences in e_{ovw} and e_{svw}. The first, with the simulated BTC trailing and overlapping the observed, is shown in Fig. 6. Second, an extreme case where only either the observed or simulated BTC have significant values is examined. The third scenario considers a more common situation, where the simulated BTC trails, but does not overlap the observed BTC.

With the simulated overlapping the observed BTC, e_{ovw} and e_{svw} can become very large. The amount for each approach depends on the amount of overlap, the primary difference being that e_{svw} increase the objective function when the simulated does not match large observed concentrations, and e_{ovw} increase the objective functions when simulated values do not match the zero, or threshold concentrations. Next, consider an observed BTC similar to Fig. 5 and a simulated BTC that, for the time period during which observations were recorded, consists of a constant value equal to the threshold concentration, in this case a normalized concentration of 10^{-8} (Fig. 7). Having an initial hydraulic conductivity estimate that is incorrect by an order of magnitude produces this situation for the system simulated in this work. Weighted residuals, using OVW or SVW, mimic the shape of the observed BTC but e_{ovw} are quite small because there are no negative residuals: the simulated BTC is flat for the time period during which observations were recorded. If the situation is reversed, where the observed BTC is a constant threshold value and the simulated BTC resembles the simulated BTC in Fig. 5, the above comments would apply to e_{svw}. However, it is far less likely that parameter estimation will be attempted when there are no significant observed concentrations, while the former situation probably occurs more frequently than most investigators care to recall.

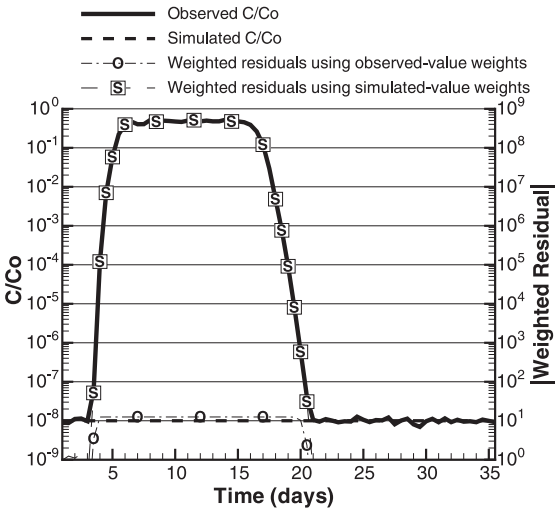

Fig. 7. Observed and simulated breakthrough curves, without any significant simulated values, and weighted residuals using observed- and simulated-value weighting. Simulated-value weighted residuals overlay the observed breakthrough curve. Observed-value weighted residuals do a poor job of reflecting the difference between observed and simulated values. If the situation is reversed, with no significant observed values and a significant simulated breakthrough curve, simulated-value weighted residuals do a poor job of reflecting the difference between observed and simulated values.

The third scenario, with the simulated BTC trailing but not overlapping the observed BTC illustrates only a slight advantage to using SVW (Fig. 8). For example, decreasing the transport rate shifts the simulated BTC curve to the right, further from the observed BTC, but decreases the e_{ovw} contribution to the objective function as the simulated BTC is shifted beyond the observation period, which for Fig. 8 would mean later than 50 days. The same decrease in transport rate would have minimal effect on e_{svw} contributions to the objective function, the majority of which are determined by the mismatch where observed concentrations are significant.

Individual circumstances may determine which approach is best for weighting residuals. In general, the arguments for using SVW become more significant when considering all aspects of sensitivity analysis and parameter estimation, as summarized in Table 2. Regardless the weighting method the two scenarios presented also tend to reiterate the benefits of using temporal-moments to supplement or replace individual conservative-transport observations: the moments provide feedback even when the observed and simulated BTCs do not overlap.

3.5. Parameter estimation scaling factor

The potential disparity between the net contribution to the objective function of fixed-weight (Eq. (13)) and variable-weight (Eq. (14)) residuals apparently defeated the purpose

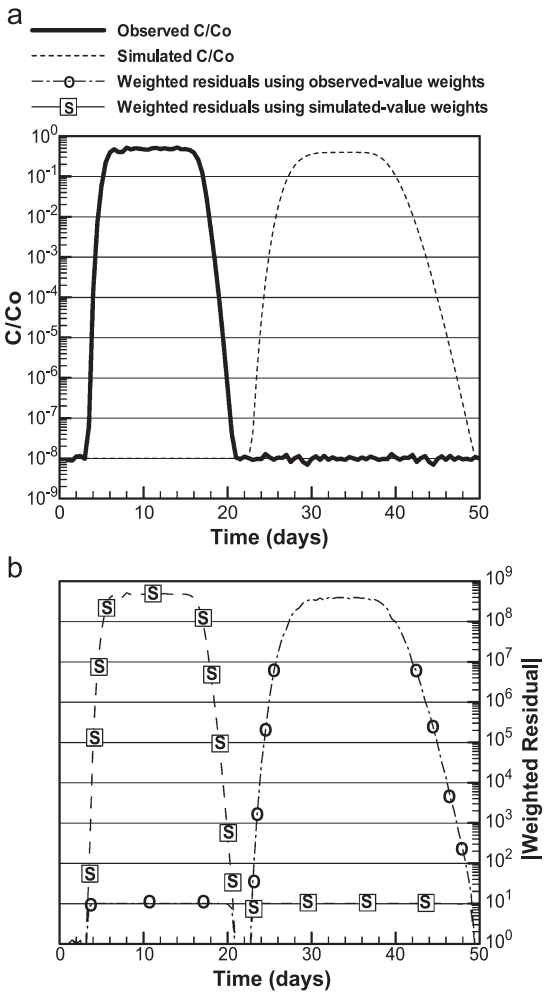

Fig. 8. (a) Simulated breakthrough curves trailing but not overlapping the observed breakthrough curve, and (b) the resulting weighted residuals using observed- and simulated-value weighting. Observed- and simulated-value weighting produces similar weighted residuals, however, decreasing the transport rate so that the simulated breakthrough curve shifts to the right and beyond the period of observations decreases the total observed-value weighting weighted residuals while having no significant impact on simulated-value weighting weighted residuals.

of the parameter-estimation scaling factor. Beginning with the first parameter-estimation iteration, χ_{r-1} tended to over-compensate, and at each successive iteration under- or over-scaled the contribution of the fixed- or variable-weight residuals by a similar factor (Fig. 9). The magnitude of χ_{r-1} and the potential for dramatic between-iterations oscillations overshadowed any benefits from scaling. This illustrates the potential benefits of damping χ_{r-1}. The tendency for χ_{r-1} to over compensate was addressed by using a fixed value of χ_{r-1}=1.0.

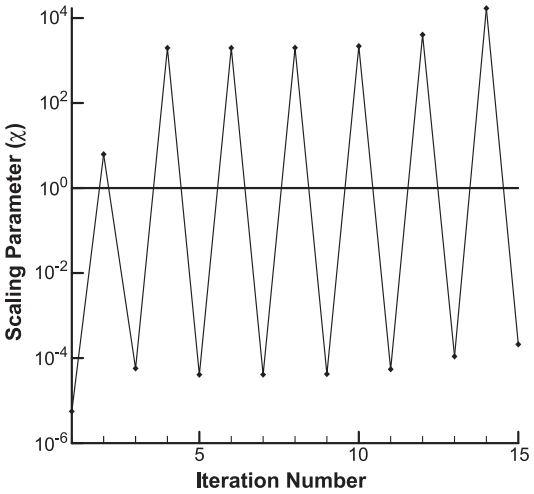

Fig. 9. Oscillations of the parameter-estimation scaling factor (χ_{r-1}) with successive iterations of the parameter estimation. The value of χ_{r-1} adjusts the relative emphasis on the fixed- and variable-weight residuals, which in this work are heads, flows and conservative-transport BTC moments, and the virus transport concentrations, respectively.

3.6. Sensitivity analysis and parameter estimation summary

Complete sensitivity-analysis and parameter-estimation results are presented in Barth and Hill (in review), and are discussed briefly in this section. This discussion is to provide insight to the potential of the methods described in this paper.

The css for the system evaluated indicate that the observations provide the most information for estimating hydraulic conductivity, porosity and the sorption rate (Fig. 3). The observations provide the most information for hydraulic conductivity and porosity primarily because both the conservative and virus concentrations provide information for these two parameters, and because the system is advection dominated.

Correlation between pairs of parameters was evaluated prior to any parameter-estimation attempts and extreme correlation between two pairs was identified: between θ and K, and between β and $\lambda 1$. The high correlation between β and $\lambda 1$ is expected given their role in Eq. (1a). Considering the coupling between C and $\bar{C}$ in Eqs. (1a) and (1b), for some sets of parameters the correlation probably depends on other parameter values, with K_d being likely. The high correlation between θ and K is expected given their role in Eq. (1c): the non-equilibrium sorption term of Eq. (1a) provides the only opportunity for θ and K to be identified uniquely. The presence of extreme parameter correlation between pairs of parameters indicates that the system evaluated does not need the full range of each and every parameter to characterize the full range of response. This notion can be extended beyond individual pairs of parameters to groups of parameters and associated dimensionless terms such as the Damkohler number (D), the ratio of characteristic residence time to characteristic reaction time. For the system analyzed, sorptive–reactive transport observations resulting from combinations of parameters, including θ, K, and β, that produce the same value of D will not provide any new information. Evaluating

correlation between multiple parameters in this system demonstrated this: correlation between K and β was as high as 0.99 when correlation coefficients were calculated for all parameters simultaneously. The extreme correlation between K and β is not evident with a pairwise evaluation of parameter correlation since other parameters in D will be fixed during the calculations. As for any parameter correlation coefficient, model nonlinearity can make parameter correlation coefficients change significantly for different parameter values (Poeter and Hill, 1998) and the correlations measured for this parameter set may change significantly for different parameter values.

Given the less than two orders of magnitude range of css for the parameters (Fig. 3), if there was not any extreme parameter correlation, it should be possible to estimate all parameters (Hill, 1998, p. 38). The existing extreme parameter correlation thwarted attempts to estimate all parameters simultaneously. Successful parameter estimation required that two parameter values be assigned prior information or be fixed at assigned values. As suggested by Hill (1998), the two approaches produce virtually the same parameter values. The parameters $\lambda 1$ and θ were fixed: $\lambda 1$ was chosen because it is much less sensitive and independent determination of $\lambda 1$ from laboratory data is more likely while θ was fixed because in unconsolidated deposits field data commonly constrain its value within a narrower range than can be achieved for K. Two parameter-estimation runs, one estimating all parameters, and the other fixing the two parameters, produced the same small value of the objective function for significantly different final parameter values, demonstrating the impact of extreme parameter correlation through the existence of multiple minima when all parameters are estimated. Two final parameter-estimation runs starting from significantly different initial values, with both $\lambda 1$ and θ fixed, produced the same parameter estimates suggesting that with the two parameter values fixed, a unique minimum is defined.

4. Conclusions

Adoption of the strategies presented in this work improved the potential for calculating accurate virus-transport parameter sensitivities and successfully performing parameter estimation using widely applicable perturbation methods. The results of this work show that when using perturbation methods to calculate sensitivities on field data sets with sharp concentration fronts it is possible to improve virus-transport parameter sensitivity analysis and estimation by (1) using alternative methods of representing observations, (2) examining the transport simulation model transport-step-size sensitivity as an indication of the threshold for parameter-sensitivity significance, (3) selecting an appropriate observation-weighting approach, and (4) determining whether the parameter-estimation scaling factor improves the regression. Based on the circumstances evaluated, this work produced the following conclusions: (1) moments of conservative transport observations provide a robust form of information for sensitivity analysis and parameter estimation, (2) the importance of the transport-step size sensitivity is comparable to several of the parameters controlling sorption and inactivation, indicating the potential for numerical variability to degrade calculated-sensitivity and parameter-estimate accuracy, (3) simulated-based weighting typically provides an advantage over observed-based weight-

ing, and (4) oscillations of the parameter-estimation scaling factor precludes its use to improve convergence.

Acknowledgements

Funding for this research was provided through the National Academy of Sciences', National Research Council's Research Associateship Program in collaboration with the United States Geological Survey's National Research Program. Comments and suggestions from Tarek Saba, Hsin-Chia Chao, Karen MacClune, Albert J. Valocchi and two anonymous reviewers helped to strengthen the manuscript and are greatly appreciated.

References

Anderman, E.R., Hill, M.C., 1999. A new multistage groundwater transport inverse method: presentation, evaluation, and implications. Water Resour. Res. 35 (4), 1053–1063.

Bales, R.C., Li, S., Yeh, T.-C.J., Lenczewski, M.E., Gerba, C.P., 1997. Bacteriophage and microsphere transport in saturated porous media: forced-gradient experiment at Borden, Ontario. Water Resour. Res. 33 (4), 639–648.

Bard, Y., 1974. Nonlinear Parameter Estimation. Academic, Orlando, FL.

Barlebo, H.C., Hill, M.C., Rosbjerg, D., Jensen, K.H., 1998. Concentration data and dimensionality in groundwater models: evaluation using inverse modeling. Nord. Hydrol. 29, 149–178.

Barth, G.R., and Hill, M.C., in review. Parameter and observation importance in modeling virus transport in saturated systems—investigations in a homogenous system, J. Contam. Hydrol.

Barth, G.R., Illangasekare, T.H., Rajaram, H., 2003. The effect of entrapped nonaqueous phase liquids on tracer transport in heterogeneous porous media: laboratory experiments at the intermediate scale. J. Contam. Hydrol. 67, 247–268.

Campbell-Rehmann, L.L., Welty, C., 1999. Stochastic Analysis of virus transport in aquifers. Water Resour. Res. 35 (7), 1987–2006.

Carrera, J., Neuman, S.P., 1986. Estimation of aquifer parameters under transient and steady-state conditions: 1. Maximum likelihood method incorporating prior information. Water Resour. Res. 22 (2), 199–210.

Corapcioglu, M.Y., Haridas, A., 1984. Transport and fate of microorganisms in porous media: a theoretical investigation. J. Hydrol. 72, 149–169.

Dennis, J.E., Schnabel, R.B., 1996. Numerical Methods for Unconstrained Optimization and Nonlinear Equations. Society for Industrial and Applied Mathematics, Philadelphia.

Draper, N.R., Smith, H., 1998. Applied Regression Analysis, 3rd ed. John Wiley and Sons, New York.

Freeze, A.R., Cherry, J.A., 1979. Groundwater. Prentice-Hall, New Jersey.

Gorelick, S.M., Evans, B., Remson, I., 1983. Identifying sources of groundwater pollution: an optimization approach. Water Resour. Res. 19 (3), 779–790.

Harbaugh, A.W., McDonald, M.G., 1996. User's Documentation for MODFLOW-96®, an update to the U.S. Geological Survey Modular Finite-Difference Ground-Water Flow Model. U.S. Geological Survey Open-File Report, 96–485.

Harvey, C.F., Gorelick, S.M., 1995. Mapping hydraulic conductivity: sequential conditioning with measurements of solute arrival time, hydraulic head, and local conductivity. Water Resour. Res. 31 (7), 1615–1626.

Hill, M.C., 1990. Preconditioned conjugate-gradient 2 (PCG2), a computer program for solving ground-water flow equations. U.S. Geological Survey Water-Resources Investigations Report 90–4048, 43 p.

Hill, M.C., 1998. Methods and guidelines for effective model calibration, U.S. Geological Survey Water Resources Investigation Report, 98–4005, 90 p.

Hill, M.C., Tiedeman, C.R., 2003. Weighting observations in the context of calibrating groundwater models. In: Kovar, K., Hrkal, Z. (Eds.), Calibration and Reliability in Groundwater Modelling: A Few Steps Closer to Reality, pp. 196–204.

James, F., 1994. RANLUX: a FORTRAN implementation of the high-quality pseudorandom number generator of Luscher. Comput. Phys. Commun. 79, 111–114.

Keider, A., Rosbjerg, D., 1991. A comparison of four inverse approaches to groundwater flow and transport parameter identification. Water Resour. Res. 27 (9), 2219–2232.

Kinzelbach, W., Schafer, W., Herzer, J., 1991. Numerical modeling of natural and enhanced denitrification processes in aquifers. Water Resour. Res. 27 (6), 1123–1135.

Poeter, E.P., Hill, M.C., 1997. Inverse models: a necessary next step in ground-water modeling. Ground Water 35 (2), 250–260.

Poeter, E.P., and Hill, M.C., 1998. Documentation of UCODE, a computer code for universal inverse modeling: U.S. Geological Survey Water-Resources Investigations Report, 98–4080, 116 p.

Schijven, J.F., Hoogenboezem, W., Hassanizadeh, S.M., Peters, J.H., 1999. Modeling removal of bacteriophages MS2 and PRD1 by dune recharge at Castricum, Netherlands. Water Resour. Res. 35 (4), 1101–1111.

Seber, G.A.F., Wild, C.J., 1989. Nonlinear Regression. Wiley, New York, NY. 768 pp.

Shapiro, A.M., Cvetkovic, V.D., 1988. Stochastic analysis of solute arrival time in heterogeneous porous media. Water Resour. Res. 24 (10), 1711–1718.

Sun, N.-Z., 1994. Inverse Problems in Groundwater Modeling. Kluwer, The Netherlands.

Tebes-Stevens, C.L., Valocchi, A.J., 2000. Calculation of reaction parameter sensitivity coefficients in multicomponent subsurface transport models. Adv. Water Resour. 23 (6), 591–611.

Tim, U.S., Mostaghimi, S., 1991. Model of predicting virus movement through soils. Ground Water 29 (2), 251–259.

Valocchi, A.J., Malmstead, M., 1992. Accuracy of operator splitting for advection–dispersion–reaction problems. Water Resour. Res. 28 (5), 1471–1476.

Van Rooy, D., Keidser, A., Rosbjerg, D., 1989. Inverse modeling of flow and transport. In: Abriola, L. (Ed.), Groundwater Contamination, vol. 185. IAHS Publication, pp. 11–23.

Wagner, B.J., Gorelick, S.M., 1986. A statistical methodology for estimating transport parameters: theory and applications to one-dimensional advective–dispersive systems. Water Resour. Res. 22 (8), 1303–1315.

Wagner, B.J., Gorelick, S.M., 1987. Optimal groundwater quality management under parameter uncertainty. Water Resour. Res. 23 (7), 1162–1174.

Yates, M.V., 1990. The use of models for granting variances from mandatory disinfection of ground water used as a public water supply, EPA Report EPA/600/2-90/010, 12 p.

Yeh, W.-G., 1986. Review of parameter identification procedures in groundwater hydrology: the inverse problem. Water Resour. Res. 22 (2), 95–108.

Zheng, C.M., 1998. A Modular Three-Dimensional Multispecies Transport (MT3DMS) Model, Release DoD_3.00.A, Prepared for the Waterways Experiment Station. U.S. Army Corps of Engineers.

Zheng, C.M., 2000. Personal Communication.

Zheng, C., Bennett, G.D., 2002. Applied Contaminant Transport Modeling, 2nd edition. Wiley, New York. 621 pp.